

# Inversion of Source Parameters and Site Effects from Strong Ground Motion Records using Genetic Algorithms

by Aaron Moya, Jorge Aguirre, and Kojiro Irikura

**Abstract** The low-frequency flat levels and corner frequencies of the aftershocks of the Kobe earthquake, together with the site effects of the recording stations, are inverted by using genetic algorithms. All records were corrected by the quality factor,  $Q$ , of propagation-path, and for each aftershock, a different omega-squared model was assumed such that the low-frequency flat levels and corner frequencies would minimize the standard deviation of the site effects at all stations. It was observed that site effects for rock sites showed significant amplification at high frequencies. This amplification was found to correlate with spectral ratios of records located at 70-m depth and at the surface for one of the stations. After estimating the seismic moment and the stress drop, it was observed that the relation of the seismic moment,  $M_0$ , versus the corner frequency,  $f_0$ , followed the scaling law  $M_0 \propto f_0^{-3}$ . Large values of stress drop were found around asperities on the fault zone and at depth.

## Introduction

Although the calculation of source parameters such as the seismic moment and stress drop is a simple procedure, it remains not a trivial task for at least two significant reasons. The first one is the contamination of the signal by the path and site effect. Conventionally, site effects are estimated relative to that for a rock site station, but the use of relative estimates introduces some bias at the time of choosing the reference site. In addition to that, recent investigations (Archuleta and Steidl, 1998; Steidl *et al.*, 1996) have shown that rock sites are not completely void of amplification at the surface. The second reason is the reading of the low-frequency flat levels and corner frequencies from the displacement spectra. In most cases, these readings are done by eye, which makes the result subjective. A small variation in the value of the corner frequency would strongly affect the result for the stress drop.

We have used genetic algorithms (GA) as an alternative means to invert the source spectra of the earthquakes and the site effects of the stations. The inversion starts by choosing a Brune's (1970) source model for each aftershock. Each source model is then used to compute the site effect of the station that has recorded the earthquake. Assuming that the site effect of a station should be the same regardless of the event, GA minimizes the standard deviation of the site effects by searching for new source models. The inversion then guarantees that the flat levels and corner frequencies obtained at the end of the inversion be the ones that would correspond to the most stable site effect estimation.

## Strong Ground Motion Records and Geology of the Area

This study concentrates on the aftershock sequence of the Kobe, Japan, earthquake (Fig. 1). The  $M_w$  6.9 earthquake occurred in 1995 in the Osaka area and it ruptured a total length of approximately 45 km along the fault strike (Seki-guchi *et al.*, 1996). The mainshock triggered a series of aftershocks that were recorded by 11 strong-motion instruments. Table 1 lists the location parameters of the aftershocks considered in this study. The instruments belong to the Committee for Earthquake Observation and Research for the Kansai Area (CEORKA), and they are all velocity sensors with a 16-bit digital recording system. The sampling rate is 100 samples/sec and instrument response is flat from 0.025 to 30.0 Hz in velocity (Toki *et al.*, 1995).

Most of the instruments were located on soft sediments inside the basin area (Fig. 2) because evaluation of the ground-motion characteristics of the basin was the prime goal of CEORKA group. Only two of them were placed on rock: CHY and KBU. Studies from well-logging data and seismic profiles of the Osaka basin area (Kagawa *et al.*, 1993) indicate that the basin has roughly an oval shape that reaches a maximum depth of approximately 2.4 km toward the south (Fig. 2). The basement rock topography becomes more irregular toward the northeastern part, right below Osaka city. The western flank, location of Kobe city, is very steep, probably due to the presence of the Rokko fault system, a series of active faults that run parallel to that edge.

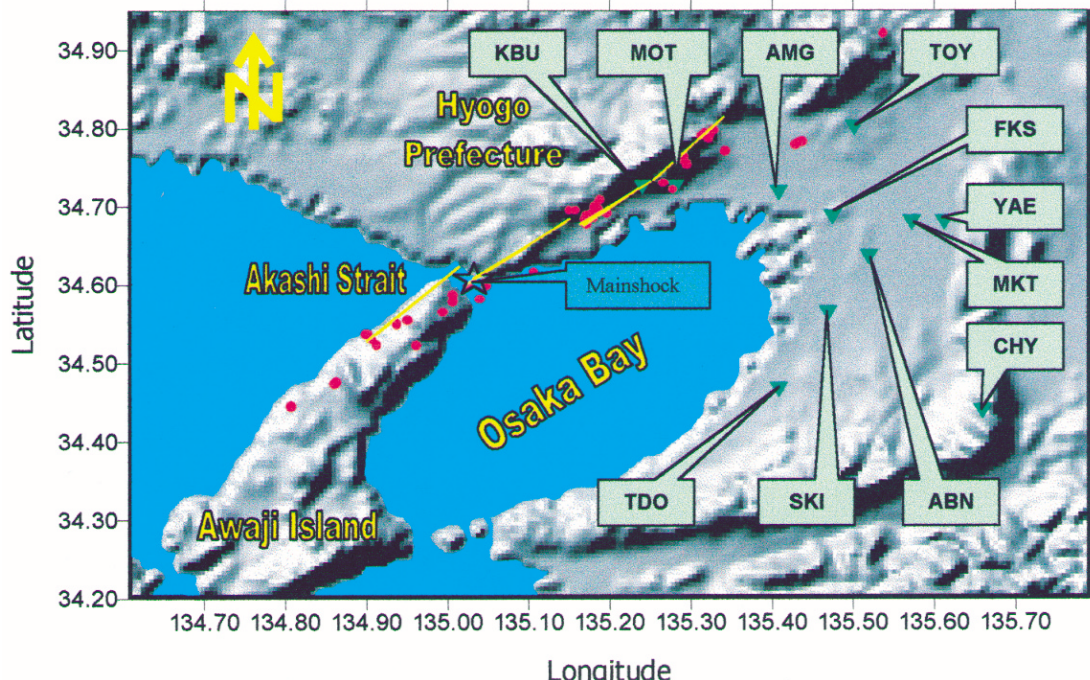


Figure 1. Location of the 1995 Kobe earthquake, aftershocks (red dots), and CEORKA stations in the Osaka area. The fault trace of the mainshock is taken from Sekiguchi *et al.* (1996).

The eastern part of the basin dips more gently toward the west, and it contains the Ikoma fault, which is reverse type with its fault plane dipping toward the east (Research Group for Active Faults of Japan, 1991).

The superficial geology of the CEORKA sites is summarized in Table 2. Also, geotechnical borehole results for the first 30 m of sediments below the stations are shown in Figure 3. This indicates that the sediments below FKS, AMG, and YAE stations are very soft compared to the rest.

#### Fourier Spectra of the Strong-Motion Records

To estimate the Fourier spectra of the aftershocks, the records of every station were first corrected to zero baseline. We took a 3-sec time window beginning from the *S*-wave arrival time from the north-south (NS) and the east-west (EW) components. A cosine taper was then applied to data 0.5 sec before and after that window to ensure that the taper applied would not disturb the amplitude of the *S* wave. The Fourier amplitude spectrum was calculated using an FFT routine applied to the NS and EW components. Each component's spectrum was then divided by  $2\pi f$ , (*f* being the frequency) in order to get the displacement spectra. The resultant horizontal displacement spectrum was then estimated as

$$O(f) = \sqrt{(NS(f))^2 + (EW(f))^2} \quad (1)$$

where  $O(f)$  is the resultant of the Fourier displacement am-

plitude of the NS and EW components. The lowest frequency in the spectrum is 0.33 Hz. The antialias filter for the CEORKA instruments has a cutoff frequency of 30 Hz (Tokii *et al.*, 1995).

As mentioned before, only two instruments were placed on rock: KBU and CHY. In the following section, we examine the amplification at KBU site by studying the spectral ratios of two earthquakes.

#### Amplification at KBU Site from Spectral Ratios

KBU station is located in the middle of the ruptured area of the mainshock (Fig. 1). The instruments are located in a 10-m-deep tunnel in weathered granite at Kobe University campus.

Figure 4 shows the displacement spectra for selected events. It is clear that the uncorrected displacement spectra at KBU are characterized by a steep decay for frequencies higher than 4 Hz while the low-frequency spectra are mostly flat. The high-frequency decay for the event 95JAN17-13:05 is affected by amplification from 3 to 6 Hz approximately, and this can be easily recognized because that earthquake has a corner frequency at around 0.9 Hz. Figure 5 shows the displacement and acceleration spectra for another earthquake. In this particular case, it can be seen that there is significant amplification in the frequency range from 1.5 to 5 Hz observed from the acceleration spectrum. The tendency for all events to decay from 4 Hz could be caused by the site effect. This amplification becomes a real problem when try-

**Table 1**  
Location Parameters for the Aftershocks

Event	Local Date–Time	Long. (East)	Lat. (North)	Depth (km)	$M_{JMA}$
1	95JAN17-06:29	134.913	034.523	11.3	4.8
2	95JAN17-06:40	135.188	034.693	9.1	3.9
3	95JAN17-06:42	135.430	034.778	15.6	4.2
4	95JAN17-06:54	134.938	034.550	12.0	4.4
5	95JAN17-07:00	134.860	034.473	11.0	4.4
6	95JAN17-07:38	135.437	034.782	11.0	4.9
7	95JAN17-08:15	135.158	034.695	13.1	4.0
8	95JAN17-08:21	134.953	034.953	14.2	4.1
9	95JAN17-08:30	135.007	034.578	10.4	4.5
10	95JAN17-08:48	135.048	034.600	14.0	4.2
11	95JAN17-08:58	135.007	034.587	18.8	4.7
12	95JAN17-09:58	134.567	034.510	13.3	4.3
13	95JAN17-12:32	135.188	034.708	17.6	4.2
14	95JAN17-13:05	135.172	034.688	11.7	4.7
15	95JAN17-18:01	135.177	034.690	14.7	3.8
16	95JAN17-22:18	134.863	034.475	11.5	4.5
17	95JAN18-00:51	135.172	034.677	18.0	4.5
18	95JAN18-05:25	135.182	034.697	14.6	4.5
19	95JAN18-06:50	135.170	034.683	13.9	4.5
20	95JAN18-13:34	135.175	034.688	15.2	4.0
21	95JAN19-01:00	135.328	034.797	13.6	4.0
22	95JAN19-10:36	135.278	034.722	9.9	4.1
23	95JAN19-18:59	134.902	034.537	15.3	4.2
24	95JAN21-21:12	134.995	034.565	14.7	4.3
25	95JAN23-00:33	134.952	034.555	8.7	4.1
26	95JAN23-06:02	134.907	034.530	15.4	4.5
27	95JAN23-21:44	135.318	034.793	16.0	4.3
28	95JAN25-23:15	135.313	034.790	16.7	4.7
29	95JAN29-16:02	135.180	034.685	13.3	3.6
30	95FEB02-16:04	135.040	034.582	11.5	4.1
31	95FEB02-16:19	135.150	034.695	17.9	4.2
32	95FEB03-04:36	135.187	034.697	14.9	3.7
33	95FEB03-20:36	135.267	034.730	11.5	3.4
34	95FEB06-13:00	135.325	034.793	11.6	3.5
35	95FEB18-21:37	134.807	034.445	12.6	4.9
36	95MAR30-14:24	135.295	034.753	12.1	3.6
37	95APR06-10:50	135.323	034.787	12.9	4.1
38	95MAY04-05:53	135.182	034.700	13.0	3.7
39	95MAY04-17:42	134.900	034.537	16.2	4.3
40	95MAY19-20:35	135.025	034.598	20.8	4.1
41	95JUN16-07:55	135.292	034.763	11.9	3.8
42	95JUN23-22:18	135.288	034.760	11.8	3.8
43	95JUL24-03:59	135.538	034.920	14.8	4.2
44	95SEP12-06:30	135.197	034.692	15.7	3.9
45	95OCT14-02:03	135.107	034.617	16.8	4.8
46	96JAN25-20:17	135.343	034.770	13.8	3.4
47	96MAY11-14:46	134.962	034.523	10.6	4.0
48	96MAY19-14:06	135.433	034.780	14.2	3.3

ing to estimate source parameters from small earthquakes, because the site amplification tends to “hide” the aftershock’s source-originated corner frequencies.

In 1997 the Electric Company Group installed two more recorders at KBU site. One of them is 70 m deep and the other is on the surface. The new instruments had recorded only two earthquakes by the time this article was being written. Unfortunately, neither earthquake was recorded at the instrument 10-m deep in the tunnel. Figure 6 shows the spectral ratio of the signals between the record at the surface and

that at 70-m depth. According to this result, the spectrum at KBU is flat up to 1.5 Hz approximately. For frequencies higher than 1.5 Hz there is amplification. This result holds even when considering the effect of the destructive interference caused by the reflective waves from the surface. The frequency at which this interference takes place is given by

$$f = \frac{2n - 1}{4H} Vs \quad (2)$$

where  $n$  is an integer,  $Vs$  is the  $S$ -wave velocity, and  $H$  is the depth. Assuming an average  $Vs = 663$  m/sec (Table 3) and  $H = 70$  m, then  $f = 2.3$  Hz. There is no trough at 2.3 Hz from the spectral ratios shown in Figure 6.

#### GA Inversion for Source Spectra and Site Effect

To estimate the source spectra, observation needs to be corrected by propagation path and site effects. Ground motion of the  $i$ th earthquake observed at the  $j$ th receiver,  $O(f)_{ij}$ , can be represented as the multiplication of three physical parameters (Iwata and Irikura, 1988):

$$O(f)_{ij} = S(f)_i P(f)_{ij} G(f)_j, \quad (3)$$

where  $S(f)_i$  is the seismic source effect of the  $i$ th earthquake,  $P(f)_{ij}$  is the term of the propagation path from the  $i$ th source to the  $j$ th receiver, and  $G(f)_j$  is the site effect of the  $j$ th receiver. The propagation-path effect,  $P(f)_{ij}$ , has the following form assuming radiation of  $S$  waves from a point source:

$$P(f)_{ij} = R_{ij}^{-1} e^{-\pi R_{ij} f / Q(f) V_s}, \quad (4)$$

where  $R_{ij}$  is the hypocentral distance from the  $i$ th source to the  $j$ th receiver,  $Q(f)$  is the quality factor, and  $V_s$  is the  $S$ -wave velocity of the medium. Substituting (4) into (3) and solving for the source term, we obtain

$$S(f)_i = \frac{O(f)_{ij}^{corr}}{G(f)_j}, \quad (5)$$

where

$$O(f)_{ij}^{corr} = R_{ij} e^{\pi R_{ij} f / Q(f) V_s} O(f)_{ij}, \quad (6)$$

Here,  $O(f)_{ij}$  is the observed spectrum for the  $i$ th earthquake at the  $j$ th station corrected by the propagation-path effect. As can be seen, in order to recover the source spectrum, observation needs to be corrected for the propagation-path and site effect. Site effect is usually estimated by dividing the observed spectra at the sediment sites by those at the rock sites (Borchardt, 1970). This technique works under the assumption that the site effect of rock sites is flat in the frequency range of interest. However, as we showed in the previous section, that assumption does not hold for KBU

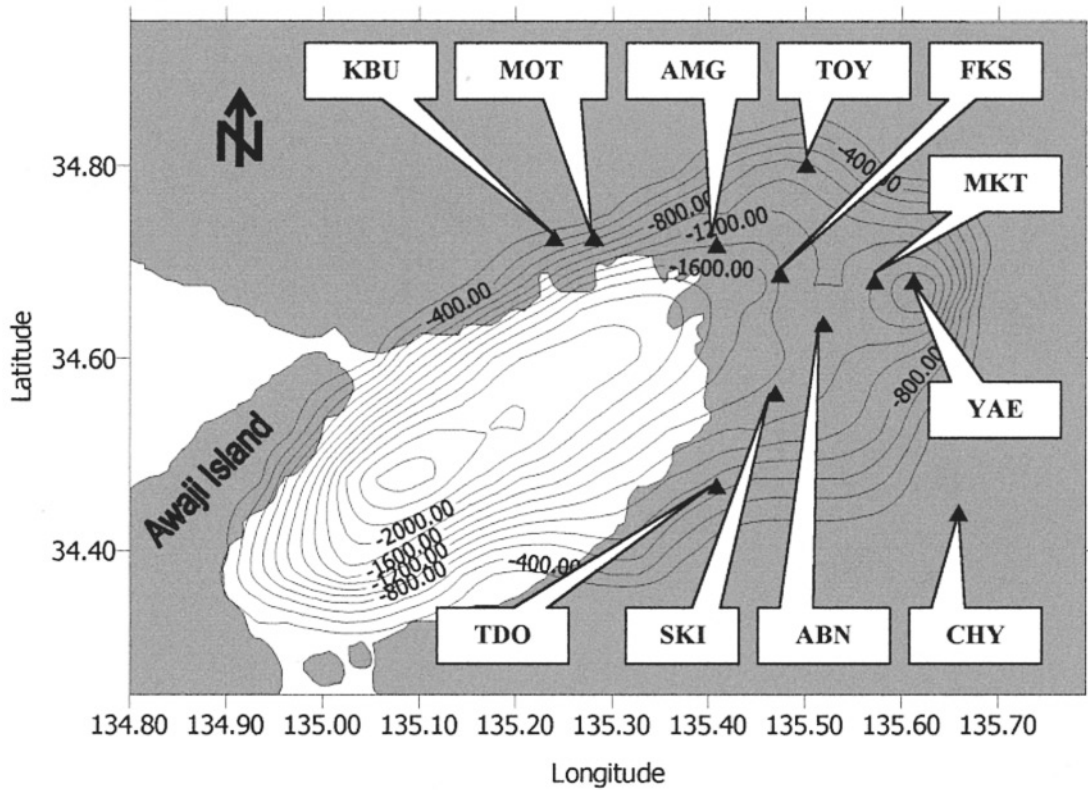


Figure 2. Osaka basin basement-rock topography and CEORKA stations. Contour lines indicate depth of the sediments in the basin in meters. The sediment cover below TDO, TOY, and SKI is thinner than that below the rest of the stations. KBU and CHY are located on granite.

Table 2  
CEORKA Stations: Location and Soil Conditions

Name	Initials	Longitude (East)	Latitude (North)	Altitude (m)	Superficial Geology
Abeno	ABN	135.519	034.636	12	Late Pleistocene deposits
Amagasaki	AMG	135.408	034.718	0	Thick Holocene deposits
Chihaya	CHY	135.659	034.439	280	Mesozoic granite
Fukushima	FKS	135.474	034.687	0	Thick Holocene deposits
Kobe University	KBU	135.240	034.725	110	Mesozoic granite
Morikawashi	MKT	135.572	034.680	1	Thick Holocene deposits
Motoyama-Kobe	MOT	135.281	034.725	25	Late Pleistocene fan deposits
Sakai	SKI	135.462	034.564	2	Thin Holocene deposits
Tadaoka	TDO	135.408	034.480	12	Thin Holocene deposits
Toyonaka	TOY	135.501	034.801	55	Pliocene deposits
Yae	YAE	135.612	034.680	3	Thick Holocene deposits

From Toki et al. (1995).

site. In addition, relative estimate would introduce serious bias by the choice of reference station.

Tsurugi *et al.* (1997) introduced a new method to estimate the site effect. After correcting the observed spectra at the rock site by the propagation path, they assumed an omega-squared model. The site effect at the *j*th station,  $G(f)_j$ , is then calculated by solving (5) for the site-effect term

$$G(f)_j = \frac{O(f)_{ij}^{\text{corr}}}{S(f)_{ir}}, \quad (7)$$

where  $S(f)_{ir}$  is the following omega-squared model (Brune, 1970) for the *i*th event obtained at the reference site, *r*. This is determined by reading a low-frequency flatlevel,  $\Omega_r$ , and a corner frequency,  $f_0$ , from the displacement spectrum re-

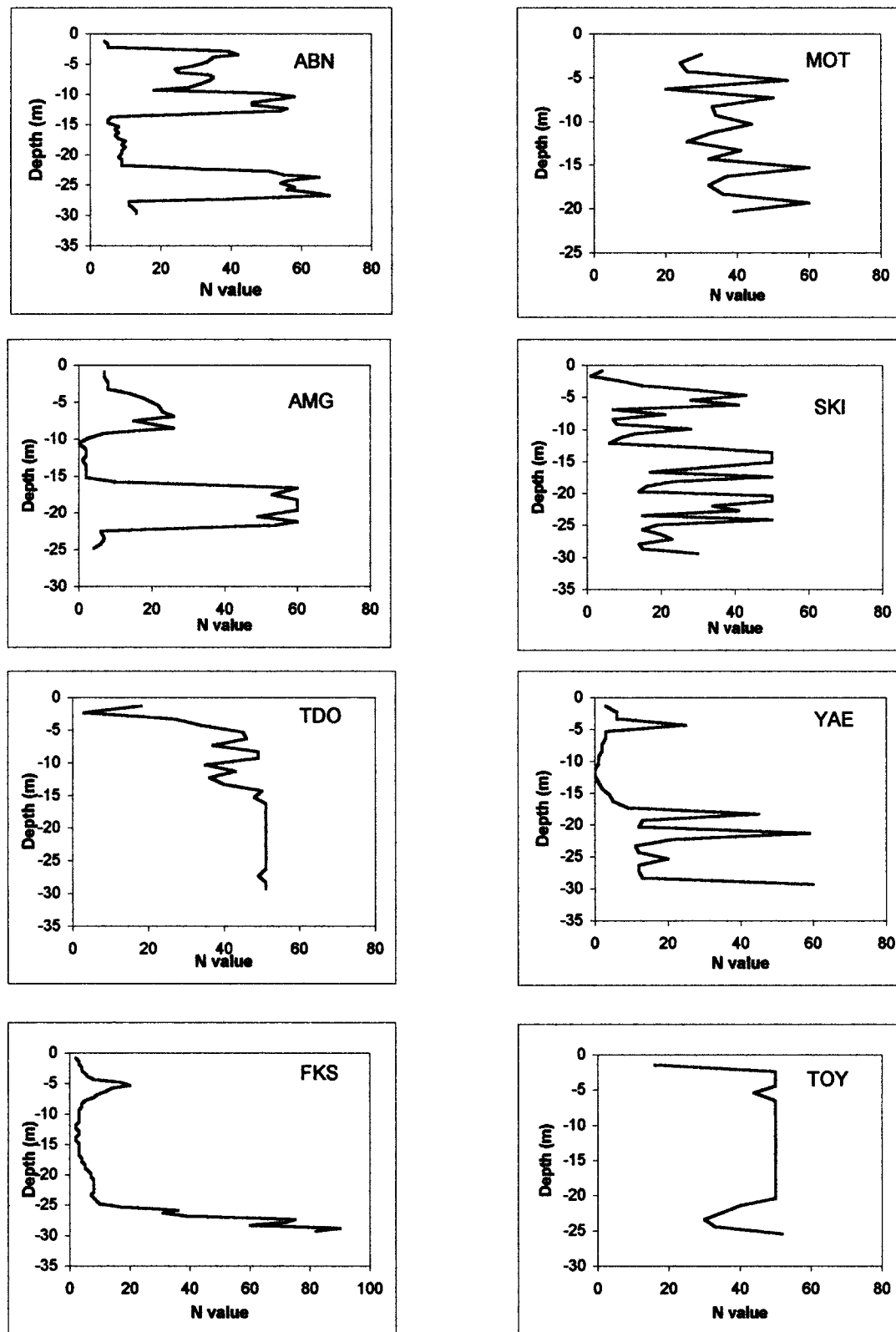


Figure 3. Blow count at the sediment site stations. A large N value corresponds to a hard soil type, small N to soft soil. Data for MKT site are missing.

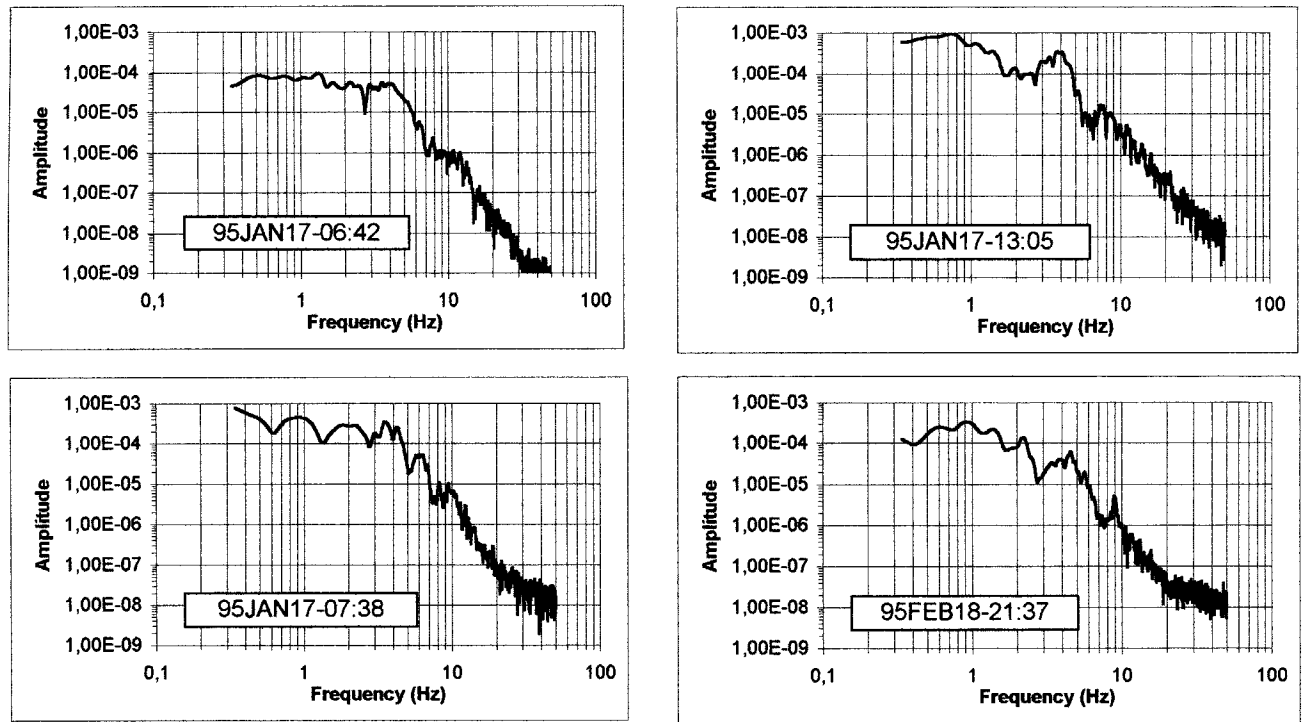


Figure 4. The “hiding” of the corner frequency by the site effects. Note how all of the four events presented here seem to have a corner frequency at around 4 Hz. This is caused by the site effect because the source-originated corner frequency is lower in every case.

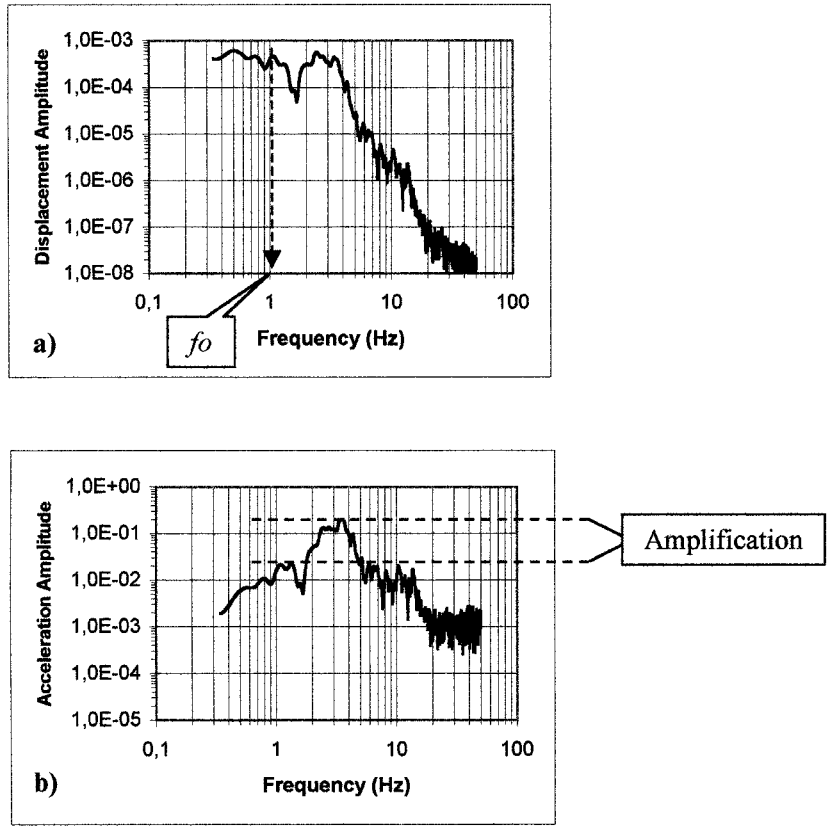


Figure 5. The (a) displacement and (b) acceleration spectrum for the 95JAN25-23:15 aftershock recorded at KBU. By looking at both spectra, it can be easily recognized that there is amplification of the signal from 1.5 to 5 Hz approximately. The corner frequency ( $f_0$ ) is not at 4 Hz as it would seem from the displacement spectrum.

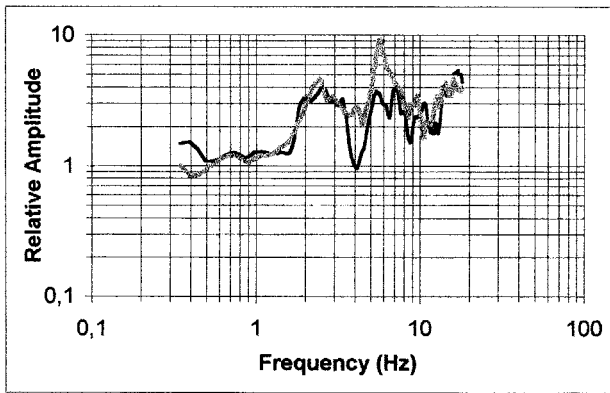


Figure 6. Spectral ratios at KBU for the 14 May 1997 earthquake (magnitude 3.2, depth 10 km) (black line) and the 12 June 1997 earthquake (magnitude 3.9, depth 15 km) (gray line) between spectra at the surface and at 70-m depth at the borehole. The spectral ratios are roughly flat for frequencies lower to 1.5 Hz.

Table 3  
Geophysical Parameter Information at KBU Borehole

Thickness (m)	Density ( $\text{g}/\text{cm}^3$ )	$P$ -wave velocity (m/sec)	$S$ -wave velocity (m/sec)
6.0	1.30	640	320
4.0	1.53	400	200
1.0	1.96	490	240
4.5	1.97	700	340
5.0	2.25	1700	590
12.0	2.08	2050	850
7.5	2.06	2250	960
12.0	2.18	2850	1120
18.0	2.12	3100	1350

corded at a rock site at the surface. The source spectrum is given by

$$S(f)_{\text{ir}} = \frac{\Omega_r/2}{1 + \left[ \frac{f}{f_0} \right]^2} \quad (8)$$

where the flat level,  $\Omega_r$ , in (8) is divided by 2 to account for the free surface effect,  $f_0$  is the corner frequency, and  $f$  is the frequency. Hand reading of flat level and corner frequency from observed spectra is not objective, and in some cases it could be prone to human error as the shape of the spectra becomes complex. The method applied in this study adopts the idea proposed by Tsurugi *et al.* (1997) with the variation that we performed a nonlinear inversion using GA to obtain the flat levels and corner frequencies.

### GA Implementation

Ever since the pioneering work of Holland (1975), GA have proven to be a powerful tool for scientists in a wide

range of fields. This searching algorithm is not constrained to solve problems following deterministic formulas. The algorithm is based on the biological principle of natural selection: only the strongest or fittest organisms survive to a given environment. In GA, data are treated as a population of individuals that experience a process of evolution through many generations in search of solutions. Each unknown parameter is a gene. In our case, we are interested in finding the low-frequency flat level of the corrected displacement spectrum at the surface,  $\Omega_0$ , and its corresponding corner frequency,  $f_0$ . Several genes make up individuals, and several individuals make up a population. Just as in nature, mutation and crossover affect the selection process. Mutation means that an entirely alien structure can be introduced to the population at any given time. In many cases, mutation helps the algorithm overcome a local minimum (solution). Crossover means that, in the same population, individuals are allowed to exchange certain characteristics, which might help them improve the performance of the species in the long run.

The data needed to be prepared for the inversion by GA. First of all, we assumed a frequency dependent  $Q(f) = 33f$  (Moya and Irikura, 1998) and  $V_s = 3.2 \text{ km/sec}$  to correct the observed spectra for the propagation path given by (6) at the CEORKA stations. After this correction, we proposed a point-source model in a similar way to (8) to estimate the site effect,  $G(f)_j$ ,

$$G(f)_j = \frac{\Omega_0/2}{1 + \left[ \frac{f}{f_0} \right]^m} \quad (9)$$

where  $m$  is 2 to meet the omega-squared model (Aki, 1967; Brune, 1970). The source term,  $S(f)_i$ , in (9) is very similar to that of (8), but this time the flat level,  $\Omega_0$ , and the corner frequency,  $f_0$ , are not obtained from hand readings from the displacement spectrum. Instead, we make use of a range in which GA is to search for the values of  $\Omega_0$  and  $f_0$ .

The upper and lower limits for the flat level are defined as follows. Considering that the low-frequency band in the rock site, KBU, is little affected by the site effect, the asymptote of the corrected amplitude level of the displacement spectrum at that station is taken as an upper limit for  $\Omega_0$ . The minimum limit is taken as a fraction of the upper limit which is  $\Omega_0/2$  or  $\Omega_0/5$  depending on the earthquake. In the case of the limits for the corner frequency, the lower limit is 0.3 and the upper limit is 5.0 Hz for all earthquakes.

Figure 7 illustrates the inversion process. The main idea is that the site effect at a given station should be the same regardless of the earthquake. GA select values for the  $\Omega_0$  and  $f_0$  from the ranges already specified to make a different source model for each earthquake. Then, the model proposed by GA divides the corresponding corrected amplitude spectrum of the event, and a site effect is calculated using (9). If, for example, we had only three earthquakes and three

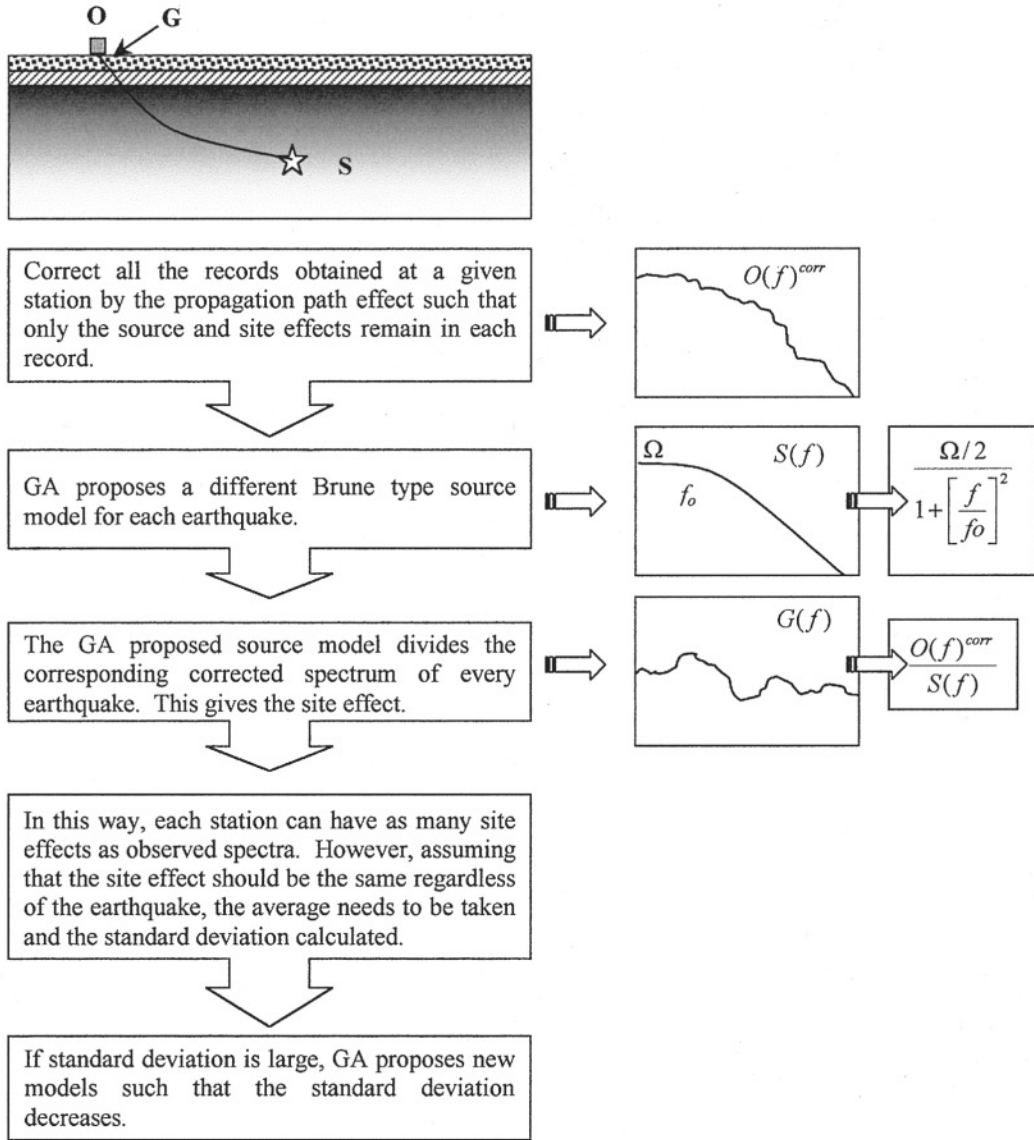


Figure 7. Outline of the GA approach to estimate the source spectrum and the site effect.

stations, then GA select three values for  $\Omega_0$  and three values for  $f_0$ . With this information we can calculate three site effects for the same station (three spectral ratios). However, the site effect should be the same regardless of the earthquake. The average and the normalized standard deviation are then calculated. The standard deviation is the value we are interested in minimizing, so the inversion continues by selecting different values of  $\Omega_0$  and  $f_0$  until a certain number of iterations (generations) is reached and the standard deviation of the site effects is minimum in every station.

In order to give equal weights to the low- and high-frequency bands, the displacement spectrum was sampled at regular intervals in the logarithmic frequency domain. This prevents the algorithm from fitting the model very well in the high frequency and poorly in the low frequency. Also, the inversion was performed using only 7 out of the 48 aftershocks listed in Table 1, because only 7 events were re-

corded by at least 10 stations. If we included more earthquakes not recorded by all stations, then the stations that contained a larger number of earthquakes would be better resolved than the rest.

### Inversion Results

We performed the inversion for a total of 200 generations and a population size equal to three times the number of genes. The residual of the normalized standard deviation is estimated as

$$\text{residual} = \sum_{k=1}^{11} \sum_{l=1}^p \delta_{lk} \quad (10)$$

where  $p$  is the total number of sampled frequencies, and  $\delta_{lk}$  is the normalized standard deviation of the site effect of the

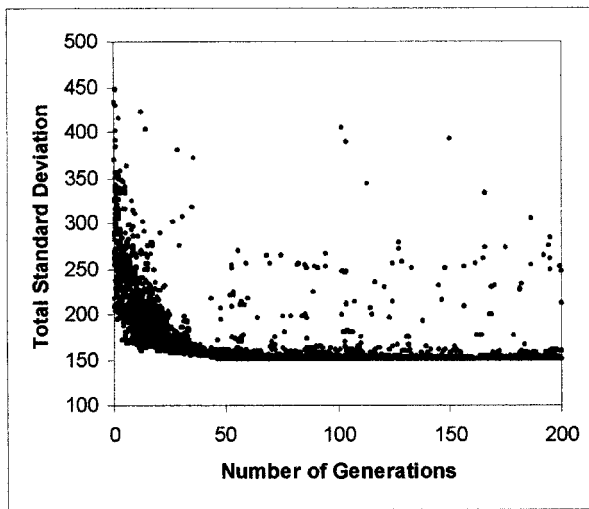


Figure 8. Evolution of the residual for 200 generations for the site effects. The residual never approaches zero, because it is the summation of the normalized standard deviations.

$l$ th frequency for the  $k$ th station. In general, the convergence of the algorithm is fast; the result does not change much after the 50th generation (Fig. 8). Since the residual is made of the summation of the normalized standard deviation for the 11 sites, it can never approach zero.

Figure 9 shows the site effects with their corresponding standard deviation. For stations located inside the basin (FKS, MTK, YAE, and AMG), the amplification is very large and the maximum values are reached at low frequencies. YAE and FKS have the fundamental frequency at 1.2 Hz, MTK at 1.7 Hz, and AMG at 1.2 Hz and 2.5 Hz approximately. The amplification at ABN and TOY is constant for the entire frequency range of interest.

As expected, the rock sites KBU and CHY are the stations that show the lowest level of amplification for frequencies below 1.5 Hz. However, for frequencies above 1.5 Hz, there is significant amplification. Both stations exhibit a peak at 4 Hz. After 4 Hz there is deamplification.

As can be seen, the amplitude of the low frequency of the site effect at KBU is two. This is theoretically acceptable for a rock site in the low-frequency range. Also, the high-frequency amplification (2–5 Hz approximately) correlates very well with the previous results from spectral ratios between signals in the borehole and on the surface (Fig. 6). The shape of the site effect for KBU also agrees with the one obtained by Tsurugi *et al.* (1997) even though the low-frequency amplification estimated by them is one at KBU. We believe this is caused by differences in the definitions of the site effects.

Normalizing the site effects in Figure 9 to KBU site, we obtain relative site effects. Figure 10 compares the relative site effects with the result from Moya and Irikura (1998). They also obtained relative estimates by using a linear inversion for the relative site effects and the  $Q$  value. The imperfect matching is expected because the number of

events used in the GA inversion is different from the one used in the linear inversion. However, the main features are the same, such as the deamplification in the high frequency for the sediment site stations and the peaks observed at FKS, MTK, and YAE stations.

Table 4 shows the flat levels and the corner frequencies for the seven events used during the inversion. The corner frequencies are smaller than the ones obtained by Tsurugi *et al.* (1997). We corrected the observed spectrum for each station by removing the propagation-path and site effects. Then we took the average and compared it to the source model as given by (8) using the flat levels and corner frequencies from Table 4. The result is shown in Figure 11. The fitting of the average source spectra to that of the one found by GA is very good considering that we are assuming a simple shape for the source in the inversion process.

### Source Parameters

Based on Brune's (1970) model, the seismic moment,  $M_0$ , of an earthquake can be derived from the flat level of the displacement spectrum given by

$$M_0 = \frac{4\pi\rho Vs^3 \Omega_0}{R_{\theta\phi}}, \quad (11)$$

where  $\rho$  and  $Vs$  are the density and the S-wave velocity of the medium, respectively,  $\Omega_0$  is the flat level of the source-displacement spectrum at a unit distance from a source centroid, and  $R_{\theta\phi}$  is the radiation-pattern coefficient. We used a density of 2.7 g/cm<sup>3</sup>, and an S-wave velocity of 3.2 km/sec, and assumed a simple form of the radiation pattern for the S waves equivalent to  $\sqrt{2}/5$  (Andrews, 1986).

The stress drop can be obtained by

$$\Delta\sigma = \frac{\rho(2\pi fo)^3 \Omega_0}{2.34 R_{\theta\phi}}, \quad (12)$$

and the source radius by

$$\text{radius} = \frac{2.34 Vs}{2\pi fo}, \quad (13)$$

Here,  $fo$  is the corner frequency and the parameters  $Vs$ ,  $R_{\theta\phi}$ ,  $\Omega_0$ , and  $\rho$  are the same ones we have previously described for (11).

The GA inversion yielded the source-spectrum flat levels and corner frequencies for seven aftershocks. In order to estimate these values for the rest of the events listed in Table 1, we first calculated their source spectra by removing the propagation-path and site effects from the observed spectra. Then, for the same earthquake, the average source spectrum was calculated.

The flat levels and corner frequencies for these events were estimated by using GA. In this case, GA were used to fit an omega-squared source model to the averaged source

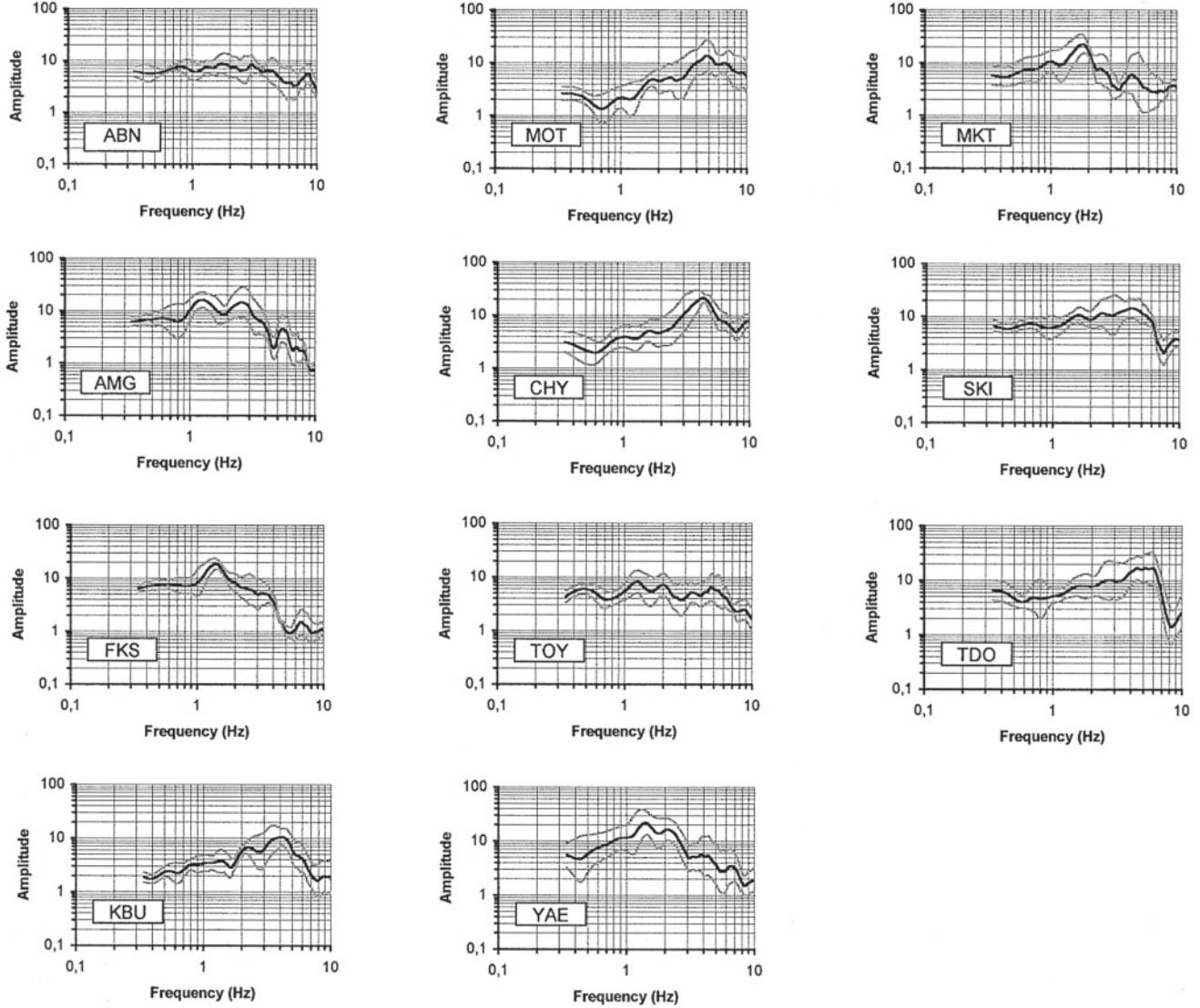


Figure 9. Site effects obtained by GA inversion of seven aftershocks. Thick black line corresponds to the average; gray lines correspond to the standard deviation. Note the amplification at the rock sites KBU and CHY in the high-frequency band.

spectrum for each individual earthquake such that the differences between the model proposed by GA and the averaged source spectrum were minimal. In other words, we searched for the best  $\Omega_0$  and  $f_0$  that minimized the summation of the error,  $\epsilon$ ,

$$\epsilon = \sum_{k=1}^p \frac{(teo_k - obs_k)^2}{\sqrt{(teo_k)(obs_k)}}, \quad (14)$$

in which  $p$  corresponds to the total number of sampled frequencies in the spectrum,  $teo_k$  corresponds to the amplitude of the theoretical source model (proposed by GA) at the  $k$ th frequency, and  $obs_k$  to the amplitude of the averaged source spectra at the  $k$ th frequency. Figure 12 shows the evolution of  $\epsilon$  for two selected earthquakes. Note that in this case the

solution approaches zero very quickly, so the inversion is set for 50 generations only. Figure 13 shows the averaged and proposed spectrum for each earthquake. The fit is generally good, although care must be taken because the error given by (14) is always positive. This causes the fitting to be computationally correct (smallest error is found) even when the matching from theory to observation would not be perfect, such is the case of event 95JUN25-17:55 in Figure 13 for which the observed spectra is not as smooth as the proposed model. These differences could also occur because the shape of the observed spectra would not adjust very well to the omega-squared model that we have assumed throughout this analysis. Events that showed these bad fittings were not considered in the determination of source parameters.

After introducing the values for  $\Omega_0$  and  $f_0$  into (10) to (12), we estimated the seismic moment, stress drop, and

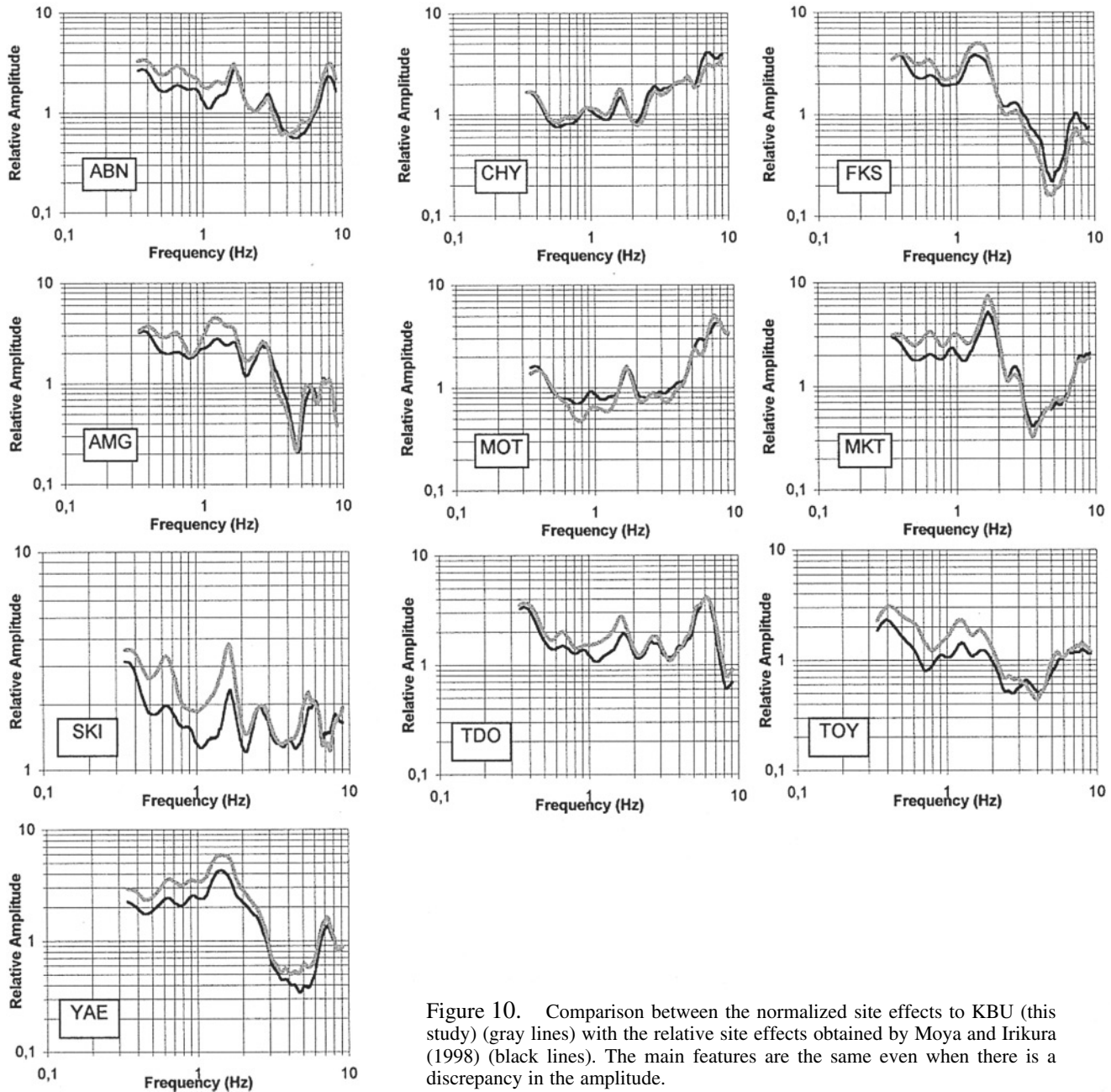


Figure 10. Comparison between the normalized site effects to KBU (this study) (gray lines) with the relative site effects obtained by Moya and Irikura (1998) (black lines). The main features are the same even when there is a discrepancy in the amplitude.

Table 4

Flat Levels and Corner Frequencies for Seven Events Obtained by GA in the First Inversion

Event	Flat Level	Corner Frequency
95JAN17-07:38	14.42	0.77
95JAN17-08:30	9.51	0.73
95JAN23-21:44	1.31	1.61
95FEB25-23:15	9.99	1.00
95FEB02-16:19	1.79	1.60
95FEB18-21:37	23.45	0.95
95OCT14-02:03	6.39	1.27

source radius, respectively. The seismic moment falls in the range of  $10^{21}$  to  $10^{24}$  dyne cm. We plotted the seismic moment versus the corner frequency (Fig. 14(a)) and found that the slope of the curve yielded a value of  $-2.7$ . In general, we can say that this relation follows the scaling law  $M_0 \propto f_0^{-3}$ . We also found that the dependence of the seismic moment on the magnitude (Fig. 14(b)) followed the equation,

$$\log[M_0] = 1.54[M_{JMA}] + 15.8, \quad (15)$$

which agreed with determinations obtained by other authors (Sato, 1979; Katsumata, 1996) for the  $M_{JMA}$  scale.

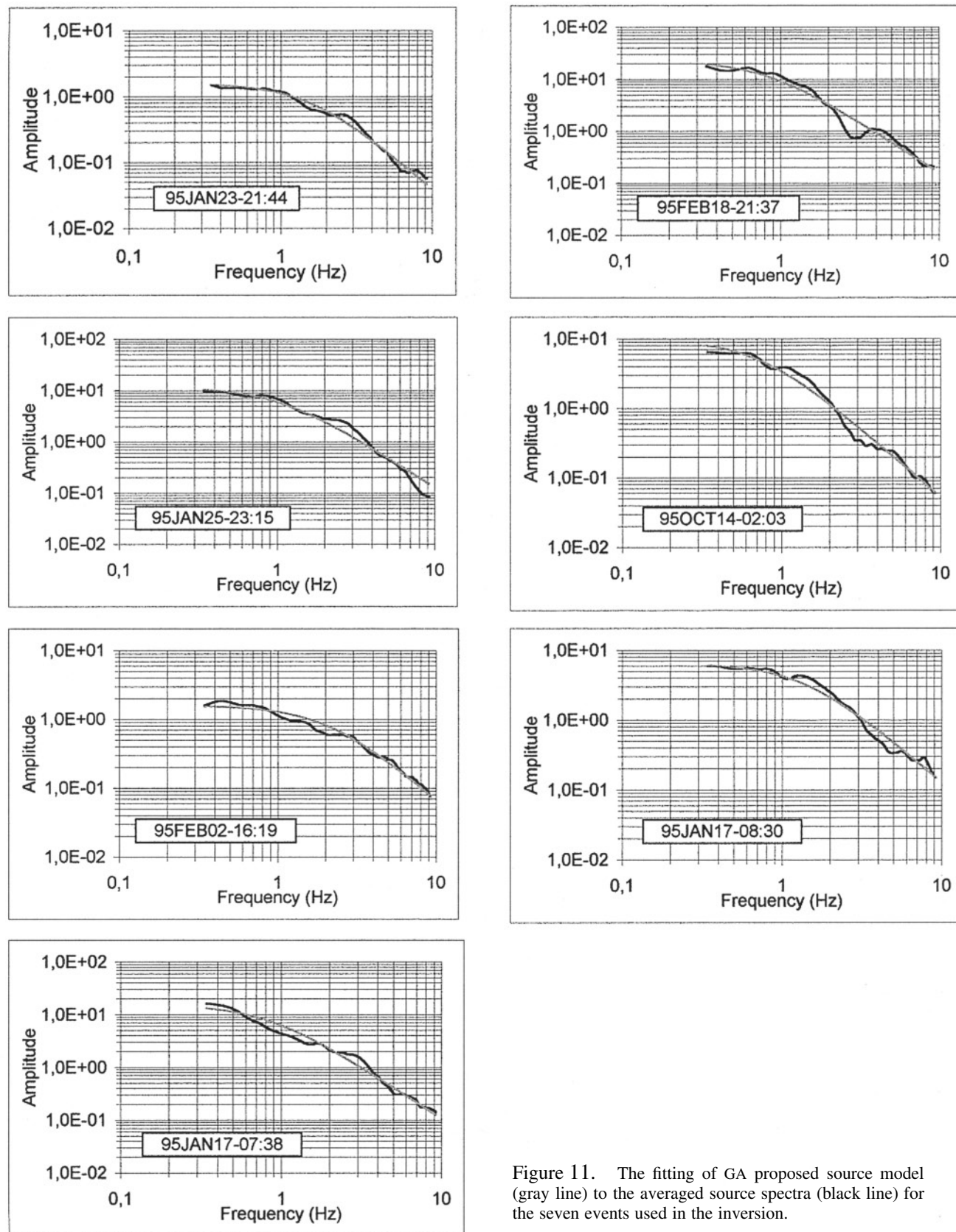


Figure 11. The fitting of GA proposed source model (gray line) to the averaged source spectra (black line) for the seven events used in the inversion.

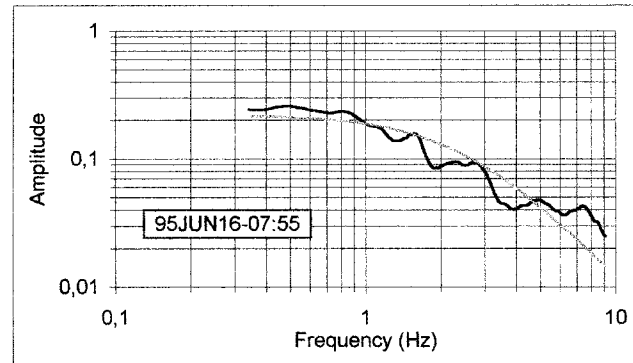
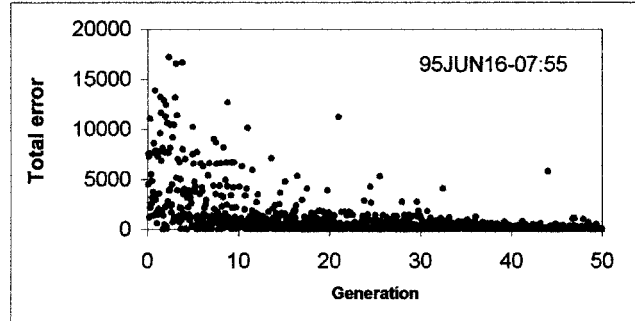
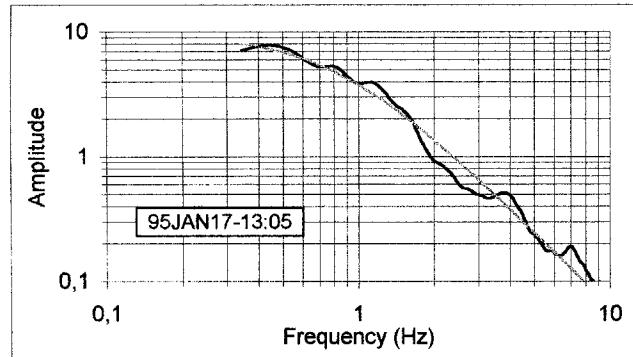
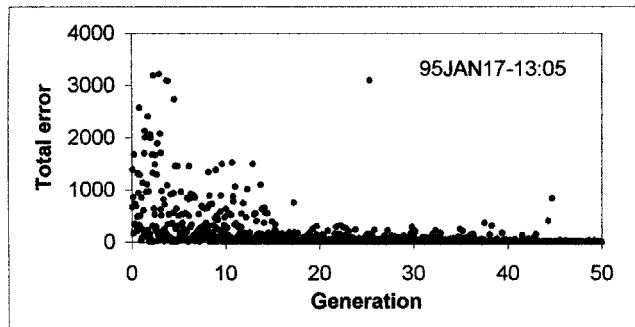


Figure 12. Evolution of the residual for two selected events. The fitting of the source model is done separately for each event.

We plotted the result for the stress drop against the seismic moment (Fig. 15(a)), the source radius (Fig. 15(b)), and the depth (Fig. 15(c)). We found no apparent dependency of the stress drop on any of the earlier parameters. However, this result could have been influenced by the site effect of the soft-sediment sites (ABN, AMG, FKS, MKT, MOT, and YAE). Even though we have made the proper correction for this factor, we should consider that the soft-sediment sites could still have a strong influence on the determination of the corner frequency and the flat levels of the aftershocks due to their amplification in the low-frequency band. Moya and Irikura (1998) noticed that the inversion of the relative site effects and  $Q$  value yielded a smaller standard deviation when they used only a limited number of stations, and that the deviation was large when they used all stations. They presumed that a very local value of  $Q$  affected the soft-sediment sites of CEORKA stations inside the basin area. For this reason, we performed another estimation of source parameters using only the hard-sediment site stations (TOY, SKI, and TDO) as well as the rock sites (KBU and CHY). These are the same stations that yielded an accurate  $Q$  value in the work by Moya and Irikura (1998). From Figure 9 we can also see that those stations are roughly flat in the low-frequency band where the corner frequency is to be found.

Since we are using a smaller number of stations this time, the number of aftershocks decreases. GA were used again search for the corner frequency and flat levels of the events recorded by the selected stations. For this new result, we plotted the stress-drop values on the hypocenters of the

Figure 13. Fitting of GA proposed source model for the two selected events. The residual from Figure 12 is low in both cases; however, sometimes the fitting of the theoretical model explains the observation very well (95JAN17-13:05) and sometimes it does not (95JUN16-07:55).

aftershocks together with the moment-release distribution of the mainshock (Sekiguchi *et al.*, 2000) in Figure 16. According to Mendoza and Hartzell (1988), it was expected that the stress drop of earthquakes at the edges of the ruptured area be higher than the ones inside it. However, events on the Awaji Island side as well as on the Kobe City side, which are outside the fault plane, show large and small values of stress drop. For those events that are inside the fault, the distribution with depth reveals a more interesting pattern. The reddish spots are associated with zones of large slip during the mainshock, which correspond to asperities. Sekiguchi *et al.* (2000) recognize the existence of three of them. The first one is located close to the starting point on the Suma fault, the second one is below Kobe City on the Suwayama fault, and the third one is located on the Nojima fault, between 2 and 10 km deep. The asperity on the Nojima fault is also the shallowest. Aftershock activity on the Nojima fault also took place at shallower depths (Nemoto *et al.*, 1996) as compared to the activity of the other faults where deeper events were recorded. Figure 17 shows the stress drop versus depth for the events, which is very scattered, but a slight indication of dependency can be recognized from it, at least for a certain group of earthquakes. On

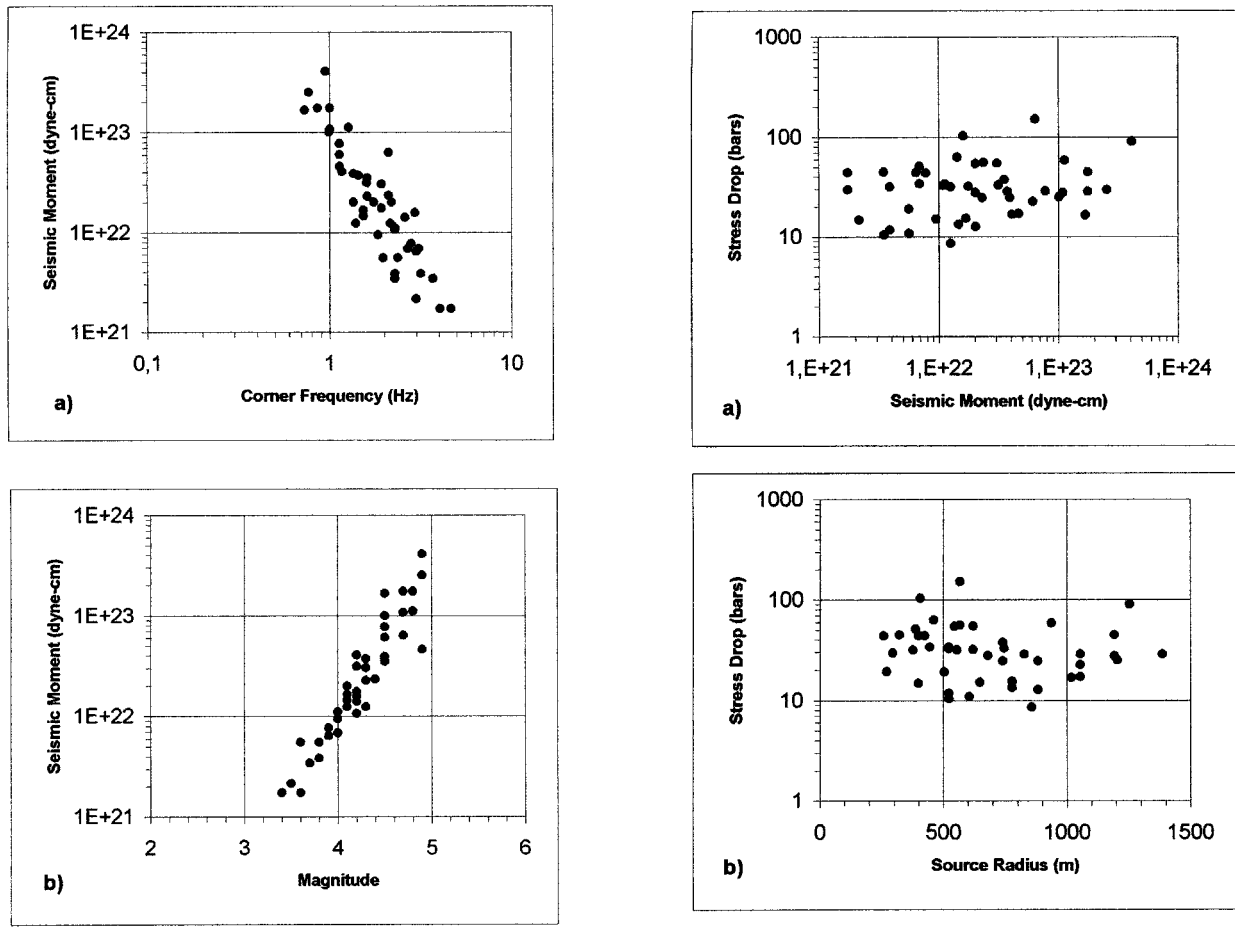


Figure 14. Result for seismic moment: (a) seismic moment versus corner frequency, (b) seismic moment versus magnitude.

the other hand, we observed no dependency of the stress drop on the seismic moment or on the source radius through this new estimation.

### Conclusions

An automated method for estimating simultaneously the site effects of stations and the source parameters of earthquakes by using genetic algorithms has been introduced. The site effects determined by GA show that stations located on soft sediments such as FKS, AMG, MKT, and YAE experience deamplification in the high-frequency range. This is in good agreement with the site-effect estimations carried out by Moya and Irikura (1998) from a linear inversion of relative site effects and  $Q$  value. Through the use of GA it has also been possible to determine the site effect for KBU site. This rock site is amplified for frequencies higher than 1.5 Hz. This result was similar to the one derived from spectral ratios of records located at the surface and at 70 m deep at that site.

We found that the majority of the aftershocks had stress-drop values lower than 50 bars, assuming the Brune's (1970)

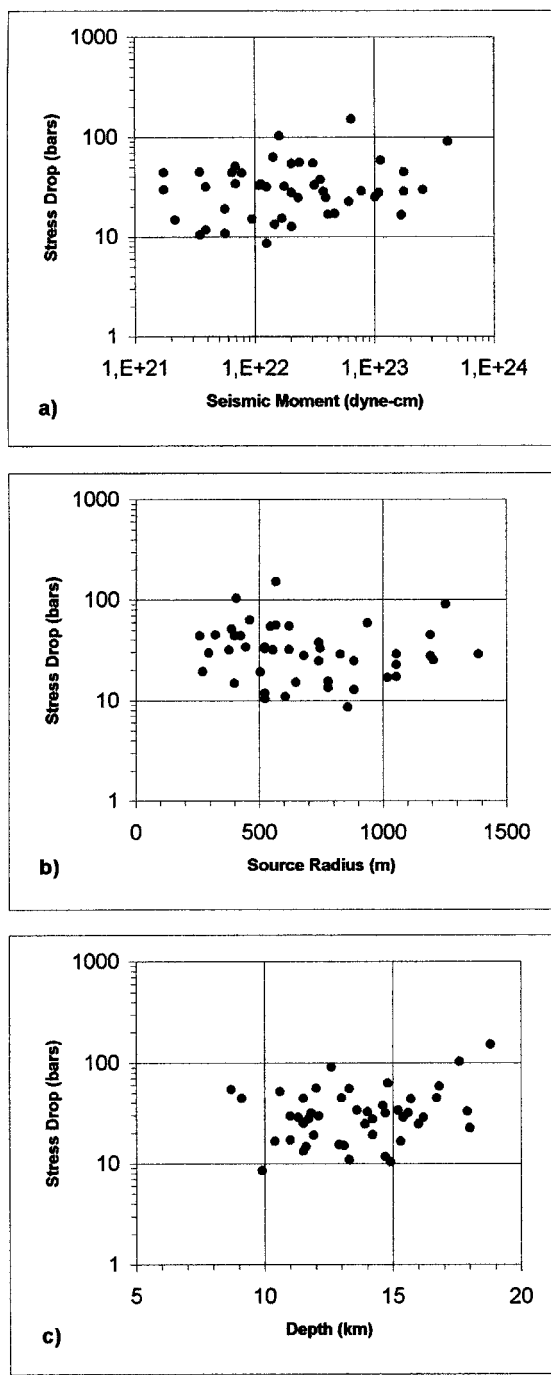


Figure 15. Result for the stress drop: (a) stress drop versus seismic moment, (b) stress drop versus source radius, and (c) stress drop versus depth.

model. It was observed that those events having stress drops above that limit were usually located around asperities and at depth. We can support this conclusion by examining the overall distribution of aftershocks on the fault plane and associating that distribution with the state of stress we obtained. Nemoto *et al.* (1996) worked on the relocation of the aftershocks that took place from 5:46 a.m. until 2:00 p.m.

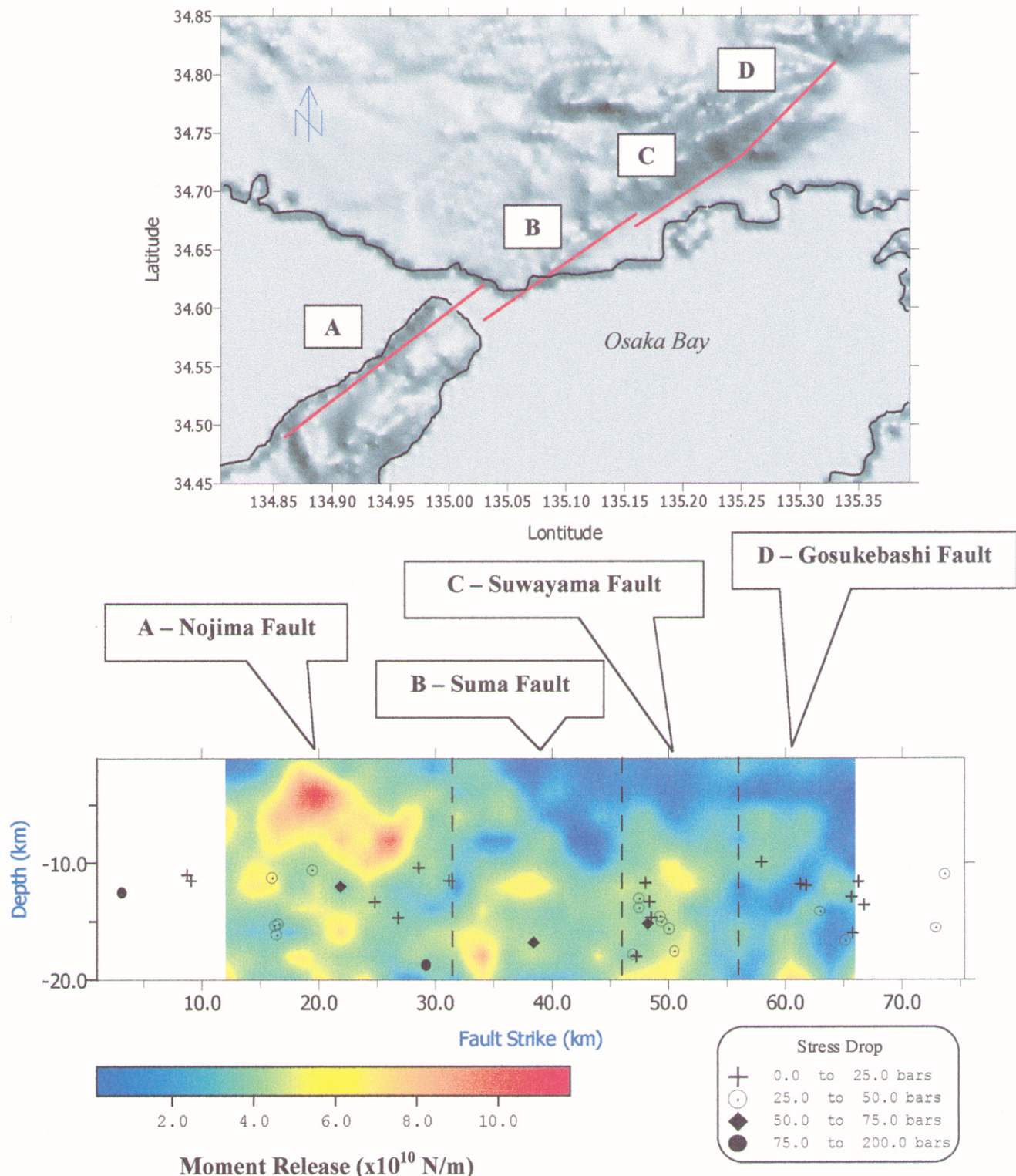


Figure 16. Stress-drop distribution along the waveform inversion result of Sekiguchi *et al.* (2000). The stress drop is systematically larger at depth and around asperities.

on 17 January. Their analysis indicates that most of the aftershocks took place between 8 and 18 km deep approximately. Only a limited number of them with magnitude

above 3.0 were located on the large Nojima asperity region. Mendoza and Hartzell (1988) have linked the occurrence to aftershocks following large earthquakes to an increase of

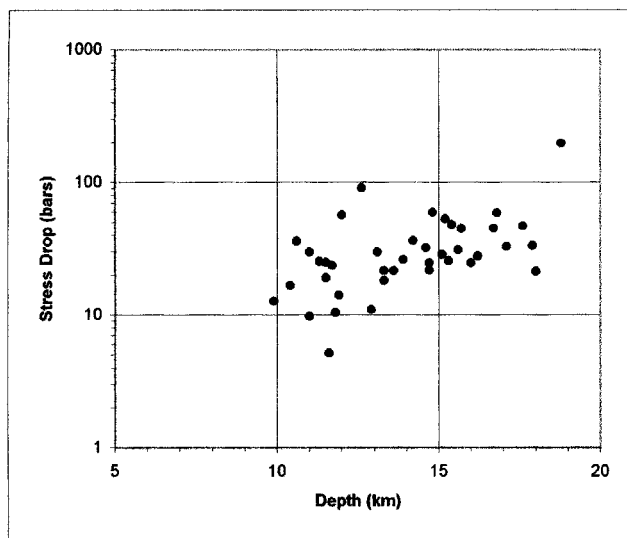


Figure 17. Stress drop versus depth for the new estimation using only five stations to calculate the corner frequency and flat levels of the aftershocks.

stress in the periphery of the zone of large slip during the mainshock. Our result for the stress drop of those events is consistent with the idea that large stress drop should be expected on those areas not ruptured by the mainshock.

Even though asperities on the other fault segments are not well constrained by the aftershock activity, we can see the common pattern that high values of stress drop are prevalent for deeper events. This is especially significant for the group of aftershocks on the Suwayama fault, which extends almost vertically from approximately 10 to 18 km and has large stress-drop values.

### Acknowledgments

We thank Anshu Jin, Haruko Sekiguchi, and Tomotaka Iwata for their helpful discussions. We also wish to thank two journal referees for their careful and critical review of the original manuscript. We are grateful to the CEORKA group for providing the strong-motion data used in this study, and to Takao Kagawa for providing the basement rock topography data of the Osaka basin. This study was completed while one of the authors (A. Moya) was a student at Kyoto University, and it was partially supported by a Grant-In-Aid for Scientific Research, No. 08248111, from the Ministry of Education, Science, Sports, and Culture of Japan. The program used for the GA inversion was GENESIS 5.0 by John J. Grefenstette.

### References

- Aki, K. (1967). Scaling law of seismic spectrum, *J. Geophys. Res.* **72**, 1217–1231.
- Andrews, D. J. (1986). Objective determination of source parameters and similarity of earthquakes of different size, *Geophysical Monographs* **37**, *6*, 259–267.
- Archuleta, R. J., and J. H. Steidl (1998). ESG studies in the United States: results from borehole arrays, in *The Effects of Surface Geology on Seismic Motion*, K. Irikura, K. Kudo, H. Okada, and T. Sasatani (Editors) Vol. 1, BAKLEMA, Rotterdam, 3–14.
- Borchardt, R. D. (1970). Effects of local geology on ground motion near San Francisco Bay, *Bull. Seism. Soc. Am.* **60**, 29–61.
- Brune, J. N. (1970). Tectonic stress and the spectra of seismic shear waves from earthquakes, *J. Geophys. Res.* **75**, 4997–5009.
- Holland, J. H. (1975). *Adaptation of Natural and Artificial Systems*, MIT Press, Cambridge, Massachusetts.
- Iwata, T., and K. Irikura (1988). Source parameters of the 1983 Japan earthquake sequence, *J. Phys. Earth* **36**, 155–184.
- Kagawa, T., S. Sawada, Y. Iwasaki, and A. Janjo (1993). On the modeling of deep sedimentary structure beneath the Osaka Plain (abstract), *Seism. Soc. Japan* **2**, 112 (in Japanese).
- Katsumata, A. (1996). Comparison of magnitude estimated by the Japan Meteorological Agency with moment magnitudes for intermediate and deep earthquakes, *Bull. Seism. Soc. Am.* **86**, 832–842.
- Mendoza, C., and S. Hartzell (1988). Aftershock patterns and mainshock faulting, *Bull. Seism. Soc. Am.* **78**, 1438–1449.
- Moya, A., and K. Irikura (1998). Attenuation and site effects in the Osaka area, Japan, in *The Effects of Surface Geology on Seismic Motion*, K. Irikura, K. Kudo, H. Okada, and T. Sasatani (Editors), Vol. 2, BAL-KEMA, Rotterdam, 469–474.
- Nemoto, H., H. Katao, E. Suzuki, Y. Yoshida, and K. Irikura (1996). The spreading of aftershocks area directly after the 1995 Hyogo-ken Nanbu earthquake, programme and abstracts, *Seism. Soc. Japan* **2**, C67 (in Japanese).
- Research Group for Active Faults of Japan (1991). *Active Faults of Japan—New Version*, University of Tokyo Press, Tokyo, 272–286 (in Japanese).
- Sato, R. (1979). Theoretical basis on the relationships between focal parameters and earthquake magnitude, *J. Phys. Earth* **27**, 353–372.
- Sekiguchi, H., K. Irikura, T. Iwata, Y. Kakehi, and M. Hoshiba (1996). Minute locating of faulting beneath Kobe and the waveform inversion of the source process during the 1995 Hyogo-ken Nanbu, Japan, earthquake using strong ground motion records, *J. Phys. Earth* **44**, 473–487.
- Sekiguchi, H., K. Irikura, and T. Iwata (2000). Fault geometry at the rupture termination of the 1995 Hyogo-ken Nanbu earthquake, *Bull. Seism. Soc. Am.* **90**, 117–133.
- Steidl, J., A. G. Tumarkin, and R. J. Archuleta (1996). What is a reference site?, *Bull. Seism. Soc. Am.* **86**, 1733–1748.
- Toki, K., K. Irikura, and T. Kagawa (1995). Strong motion records in the source area of the Hyogo-ken Nanbu earthquake, January 17, 1995, Japan, *J. Natural Disast. Science* **16**, 23–30.
- Tsurugi, M., M. Tai, K. Irikura, and A. Kowada (1997). Estimation of empirical site amplification effects using observed records, *Zisin J. Seism. Soc. Japan* **50**, 215–227 (in Japanese).
- Laboratorio de Ingeniería Sísmica  
Instituto de Investigaciones en Ingeniería  
Universidad de Costa Rica  
San José, Costa Rica  
(A. M.)
- Instituto de Ingeniería  
Ciudad Universitaria  
Apdo. Postal 70-472  
Coyoacán, C.P. 04510  
México, D. F., Mexico  
(J. A.)
- D.P.R.I., Kyoto University  
Gokasho, Uji  
Kyoto, 611-0011, Japan  
(K. I.)